AGU PUBLICATIONS

Geophysical Research Letters

RESEARCH LETTER
10.1002/2015GL066563

Key Points:
- The Vegetation-Atmosphere Coupling (VAC) index between FPAR and temperature is introduced
- The VAC index distinguishes between atmospheric and land-driven evaporative regimes
- The VAC index indicates strong coupling particularly during droughts and heat waves

Supporting Information:
- Supporting Information S1
- Figure S1
- Figure S2
- Figure S3
- Figure S4

Correspondence to:
J. Zscheischler, and S. I. Seneviratne, jakob.zscheischler@env.ethz.ch; sonia.seneviratne@ethz.ch

Citation:
Zscheischler, J., R. Orth, and S. I. Seneviratne (2015), A submonthly database for detecting changes in vegetation-atmosphere coupling, *Geophys. Res. Lett.*, *42*, 9816–9824, doi:10.1002/2015GL066563.

Received 12 OCT 2015
Accepted 4 NOV 2015
Accepted article online 10 NOV 2015
Published online 25 NOV 2015

A submonthly database for detecting changes in vegetation-atmosphere coupling

Jakob Zscheischler[1], René Orth[1], and Sonia I. Seneviratne[1]

[1] Institute for Atmospheric and Climate Science, ETH Zurich, Zurich, Switzerland

Abstract Land-atmosphere coupling and changes in coupling regimes are important for making precise future climate predictions and understanding vegetation-climate feedbacks. Here we introduce the Vegetation-Atmosphere Coupling (*VAC*) index which identifies regions and times of concurrent strong anomalies in temperature and photosynthetic activity. The different classes of the index determine whether a location is currently in an energy-limited or water-limited regime, and its high temporal resolution allows to investigate how these regimes change over time at the regional scale. We show that the VAC index helps to distinguish different evaporative regimes. It can therefore provide indirect information about the local soil moisture state. We further demonstrate how the index can be used to understand processes leading to and occurring during extreme climate events, using the 2010 heat wave in Russia and the 2010 Amazon drought as examples.

1. Introduction

The land surface is an important component of the climate system [*Seneviratne et al.*, 2010]. Through exchanges of energy and water, it is coupled with the atmosphere such that water availability on land and the (consequent) state of the vegetation have implications on near-surface weather conditions [*Koster et al.*, 2004; *Seneviratne et al.*, 2006; *Guillod et al.*, 2015]. In particular, soil moisture (SM) can influence the partitioning of incoming radiation into the sensible and latent heat fluxes at the surface and hence temperature and humidity in the lower atmosphere. Moreover, SM has direct impact on vegetation activity and hence plant transpiration [*Koster and Milly*, 1997; *Teuling et al.*, 2009], which accounts for about 65% of total evapotranspiration (ET) [*Schlesinger and Jasechko*, 2014; *Good et al.*, 2015].

The role of the land surface within the climate system varies geographically and temporally as a function of the regional SM content, such that different regimes can be distinguished [*Seneviratne et al.*, 2010]: (i) in a *wet regime*, the SM content is high, vegetation activity depends on incoming radiation, and ET is consequently *energy limited*; (ii) in a *transitional regime*, the SM content is lower, vegetation activity therefore depends increasingly on SM, and ET is consequently *water limited*; and (iii) in a *dry regime*, the SM content is very low such that vegetation is almost absent and ET is still water limited but close to zero and thus has little impact on the atmosphere.

Even though the climate in a given region is mostly characterized by a dominant evaporative regime, it may occasionally switch into another regime following, e.g., precipitation or radiation anomalies. Such transitions change the local land-atmosphere dynamics and can therefore amplify existing precipitation and temperature anomalies and consequently contribute to the persistence of extreme events such as heat waves or droughts [*Oglesby and Erickson III*, 1989; *Lorenz et al.*, 2010; *Whan et al.*, 2015] with critical impacts on ecosystems and the carbon cycle [*Reichstein et al.*, 2013; *Frank et al.*, 2015]. Whereas the prevailing regimes are well characterized [*Teuling et al.*, 2009], local regime changes before and during extreme events are mostly indirectly detected: many studies employ only precipitation and temperature data due to lacking ET and SM data [e.g., *Hirschi et al.*, 2011; *Mueller and Seneviratne*, 2012; *Quesada et al.*, 2012; *Ford and Quiring*, 2013].

As an alternative, we present here a combined analysis of global temperature and vegetation activity data and introduce a Vegetation-Atmosphere Coupling index (*VAC*). For this purpose we employ satellite-derived observations of the fraction of absorbed photosynthetically active radiation (FPAR) which constitutes a measure of photosynthetic activity [*Gobron et al.*, 2010]. FPAR is a dimensionless indicator of how much solar radiation energy in the PAR domain is absorbed by vegetation and available for photosynthesis [*Pinty et al.*, 2009].

It plays an increasingly important role in the investigation of the global biogeochemical cycles including carbon and water fluxes. For instance, FPAR has been used as independent reference for the evaluation of prognostic terrestrial ecosystem models [*Knorr et al.*, 2007]. Interannual variability of ET is strongly controlled by interannual variability of vegetation activity, in particular during the growing season [*Suzuki et al.*, 2007; *Lawrence et al.*, 2011]. Combining temperature and FPAR enables us for the first time to derive a global long-term inventory which allows to determine and detect changes in the dominant active evaporative regime at a biweekly time scale and at high spatial resolution. Previous attempts to study vegetation-atmosphere interactions usually had to rely either on process-based models or cover much shorter time spans and spatial scales. Furthermore, by exploiting the coupling between photosynthesis and the water cycle, we can indirectly gain information about the SM state in vegetated areas.

Obtaining observation-based estimates of SM and ET at the global scale over longer time spans is difficult [*Seneviratne et al.*, 2010; *Wang and Dickinson*, 2012]. Nevertheless, in recent years methodological advances and increased availability of ET and SM measurements and estimates have paved the way for the introduction of new reference data sets [*Mueller et al.*, 2013; *Orth and Seneviratne*, 2015]. In addition, new multimodel-based ET estimates are available (J. Schellekens et al., Construction and dissemination of a global water resources reanalysis data set using an ensemble of global hydrological and land surface models: The eartH2Observe tier-1 data set, submitted to *Geoscience Data Journal*, 2015). By employing these products, we can validate and further complement the above mentioned inventory with a detailed analysis of the underlying processes that modulate land-atmosphere dynamics between energy- and water-limited regimes. To illustrate the usefulness of the VAC, we investigate the 2010 heat wave in western Russia and the 2010 drought in the Amazon on a case study basis.

Moreover, we use a variety of independent data products to demonstrate the validity of conceptual depictions of the evaporative regimes.

2. Data and Methods

We use the FPAR3g product derived from the Global Inventory Modeling and Mapping Studies [*Zhu et al.*, 2013], available at 1/12° spatial and biweekly temporal resolution from July 1981 to the end of 2011. FPAR is aggregated to 0.25°, and only complete years are used (1982–2011). We use ERA-Interim temperature (T) [*Dee et al.*, 2011] interpolated to the same spatial and temporal resolution. For a comparison with ET we use two data products: (i) the LandFlux-EVAL ET product [*Mueller et al.*, 2013], available at monthly scale at 1° spatial resolution over the time period 1989–2005, and (ii) the median of reference ET simulations of seven state-of-the-art land surface models conducted within the eartH2Observe project (https://wci.earth2observe.eu, Schellekens et al., submitted manuscript, 2015). The eartH2Observe products are available at 0.5° spatial resolution from 1979 to 2012. Daily values are averaged to a biweekly time scale. In the results presented in the article the earthH2Observe ET data are used in order to maximize temporal overlap. However, results are qualitatively similar for both ET products, and anomaly time series compares well across both ET products in the overlapping time period (1989–2005), in particular in arid and semiarid areas (Figure S1 in the supporting information).

The presented Vegetation-Atmosphere Coupling (VAC) index is constructed biweekly between T and FPAR (VAC^{FPAR}) on 0.25° and T and ET (VAC^{ET}) on 0.5° spatial resolution: For each variable and each pixel we compute anomalies by subtracting the mean seasonal cycle. A percentile-based threshold is then defined based on the absolute values of each of the anomaly time series for both variables. In this paper we choose the 70th and 95th percentiles as these thresholds correspond to approximately 1 and 2 standard deviations for normally distributed data. If anomalies of FPAR (or ET) and T simultaneously exceed the threshold, they are assigned to one of four categories depending on their sign. More specifically, for each pixel and given (percentile dependent) thresholds th_T and th_{FPAR},

$$VAC^{FPAR} = \begin{cases} a & \text{if} \quad x_T < -th_T \quad \text{and} \quad x_{FPAR} < -th_{FPAR} \\ b & \text{if} \quad x_T > th_T \quad \text{and} \quad x_{FPAR} > th_{FPAR} \\ c & \text{if} \quad x_T > th_T \quad \text{and} \quad x_{FPAR} < -th_{FPAR} \\ d & \text{if} \quad x_T < -th_T \quad \text{and} \quad x_{FPAR} > th_{FPAR} \\ 0 & \text{otherwise,} \end{cases} \tag{1}$$

Table 1. Definition of the Different Classes of the Index

Sign of Anomalies		Index	SM Regime	Status	Color[a]
$T-$	FPAR/ET−	VAC_a	energy-limited	wettening, atmospheric control	blue
$T+$	FPAR/ET+	VAC_b	energy-limited	drying, atmospheric control	orange
$T+$	FPAR/ET−	VAC_c	transitional	drying, land/vegetation control	red
$T-$	FPAR/ET+	VAC_d	transitional	wettening, land/vegetation control	green

[a]For Figures 1b, 1c, 3, and 4: If the percentile-based threshold of 70% is crossed, light colors are used; if 95% are crossed, saturated colors are used.

where x_T and x_{FPAR} denote anomalies of T and FPAR, respectively. VAC^{ET} is defined accordingly by exchanging FPAR with ET. Our analyses mostly focus on VAC^{FPAR} because T and FPAR are derived from independent sources. A summary of the different classes including a short interpretation is given in Table 1. An example of the VAC^{FPAR} index and its computation based on T and FPAR anomalies at Moscow for the second half of the time period (1997–2011) is given in Figure S2. We denote the occurrence of classes a through d with VAC_a through VAC_d and omit the superscript when we refer to both FPAR and ET. We designed a permutation test where instances of VAC^{FPAR} and VAC^{ET} are shuffled 1000 times in time and co-occurrences are counted to estimate whether the instances of both indices co-occur significantly more often than expected by chance. We say VAC^{FPAR} and VAC^{ET} are co-occurring significantly more often than random at a pixel if its co-occurrence rate is higher than in 95% of the randomly shuffled cases.

For validating conceptual depictions of the evaporative regimes, we further use reconstructed SM by *Orth and Seneviratne* [2015] and net radiation by combining the NASA/Global Energy and Water Cycle Experiment Surface Radiation Budget data set and Clouds and the Earth's Radiant Energy System data [*Orth and Seneviratne*, 2015] available at 0.5° over Europe. For these data sets we aggregate daily values to biweekly time periods. Finally, evaporative fraction (EF) is computed at each biweekly time step by dividing latent heat by net radiation.

3. Results and Discussion

3.1. Illustrating Land-Atmosphere Coupling With a Novel Combination of Data Sets

Land-atmosphere coupling differs between energy- and water-limited regimes. Figure 1a depicts the feedbacks that can occur between T, ET/FPAR, and SM with precipitation (P) as a confounding factor. Changes in T translate into changes in ET/FPAR in the same direction in energy-limited regimes, whereas changes in ET/FPAR influence SM in the opposite direction. In a SM-limited regime, changes in SM affect ET/FPAR in the same direction, while ET and FPAR are negatively affecting T [*Seneviratne et al.*, 2010]. P is negatively correlated with T [*Berg et al.*, 2015] and positively with SM. Note that under certain conditions there is a positive or negative feedback between SM and P [*Taylor et al.*, 2012; *Guillod et al.*, 2015]. VAC investigates the relationship between T and ET/FPAR anomalies and is in class a or b when anomalies in T and ET/FPAR are large and have the same sign or in class c or d when anomalies have opposite signs (see also equation (1)).

It should be noted that the negative correlation of P with T is on the one hand due to a purely atmospheric covariation (cloud cover and atmospheric regime) and on the other hand to the control through the SM pathway (Figure 1a (right)). The disentangling of the two pathways can only be done exactly in a modeling framework, and previous work suggests that the SM pathway is dominant although the atmospheric pathway is not negligible [*Berg et al.*, 2015].

Figures 1b and 1c show the relation between FPAR and T anomalies in an energy-limited regime (Europe) and a water-limited regime (Australia). Points that fall in the different classes of VAC^{FPAR} are colored according to Table 1. Clearly, Europe has more incidences of classes VAC_a^{FPAR} and VAC_b^{FPAR}, while Australia has more incidences of VAC_c^{FPAR} and VAC_d^{FPAR} (see also Figures 2a and 2b).

Visualizations of the four different classes of the VAC in the context of different evaporative regimes [*Seneviratne et al.*, 2010, Figure 5] are depicted in Figure 1d. Classes a and b are representative for changes along the wet, energy-limited regime. VAC_a is related to lower T which is generally associated with the presence of clouds and precipitation [*Berg et al.*, 2015] that lead to a decrease in photosynthetic activity (and ET) and consequently can increase SM. During VAC_b on the other hand, T is higher than normal which is mostly associated with a clear sky and above normal radiation [*Berg et al.*, 2015], triggering excessive plant activity and depletion of SM. Note that VAC_a and VAC_b are associated with changes in ET, but because this is driven by changes in radiation, no significant change in the evaporative fraction (EF) occurs (horizontal arrows

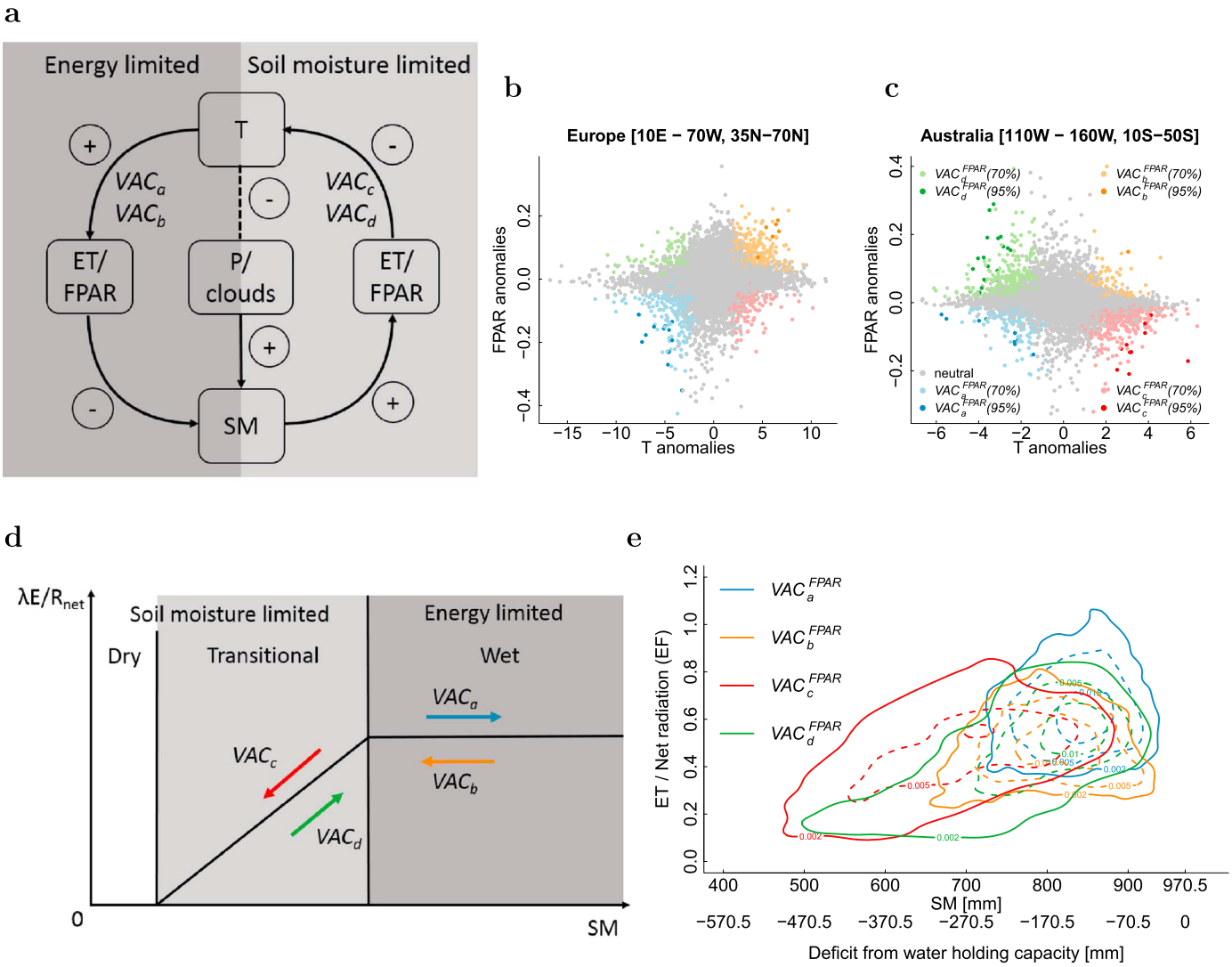

Figure 1. (a) Feedbacks between *T*, ET/FPAR, and SM in energy- and SM-limited regimes. + and − denote positive and negative correlations, respectively. *P* is precipitation. VAC_a and VAC_b are associated with strong anomalies in *T* and ET/FPAR with the same sign. VAC_c and VAC_d are associated with anomalies with the opposite signs. The dashed line between *T* and *P*/clouds corresponds to the negative atmospheric covariation between these variables. Please note that soil moisture can also affect precipitation (either positively or negatively) in some regions (see text). (b) FPAR anomalies versus *T* anomalies for 10,000 random samples in Europe. Points are colored according to the classes of VAC^{FPAR}. (c) As in Figure 1b but for Australia. (d) Alignment of the four incidences of the VAC index in the conceptual diagram of Figure 5 in *Seneviratne et al.* [2010]. (e) Contour lines of the empirical probability density of EF and SM (and SM deficit from the water holding capacity) during summer in Europe (June, July, and August (JJA), 1984–2011) for points falling in one of the four classes of VAC^{FPAR}. Solid lines indicate density levels of 0.002, whereas higher levels are drawn with dashed lines.

for VAC_a and VAC_b in Figure 1d). VAC_c and VAC_d fall in the transitional SM regime. Periods of VAC_c are characterized by plant water stress with strongly diminished photosynthetic activity, generally due to SM deficits following a lack of rain, which can enhance *T* and further reduce SM [*Seneviratne et al.*, 2006, 2010; *Miralles et al.*, 2014]. During VAC_d plant activity is increased because of above normal rainfall over dry soils, leading to increased SM and lower *T*.

While the above framework describes well the different SM regimes and their impact on ET, it has not yet been confirmed with actual data (but see *Teuling et al.* [2010] for a regional study). We will make an attempt in this direction here. For this purpose and following the availability of the employed data products we focus on summer months in Europe (JJA) and plot contour lines of the distributions between the evaporative fraction (EF) and SM for points that fall in one of the four different classes VAC_a^{FPAR} through VAC_d^{FPAR} (Figure 1e). VAC_a^{FPAR} and VAC_b^{FPAR} are associated with high SM values and no apparent relationship between EF and SM. During incidences of VAC_a^{FPAR}, EF is slightly higher than during VAC_b^{FPAR}, probably related to a nonlinear scaling

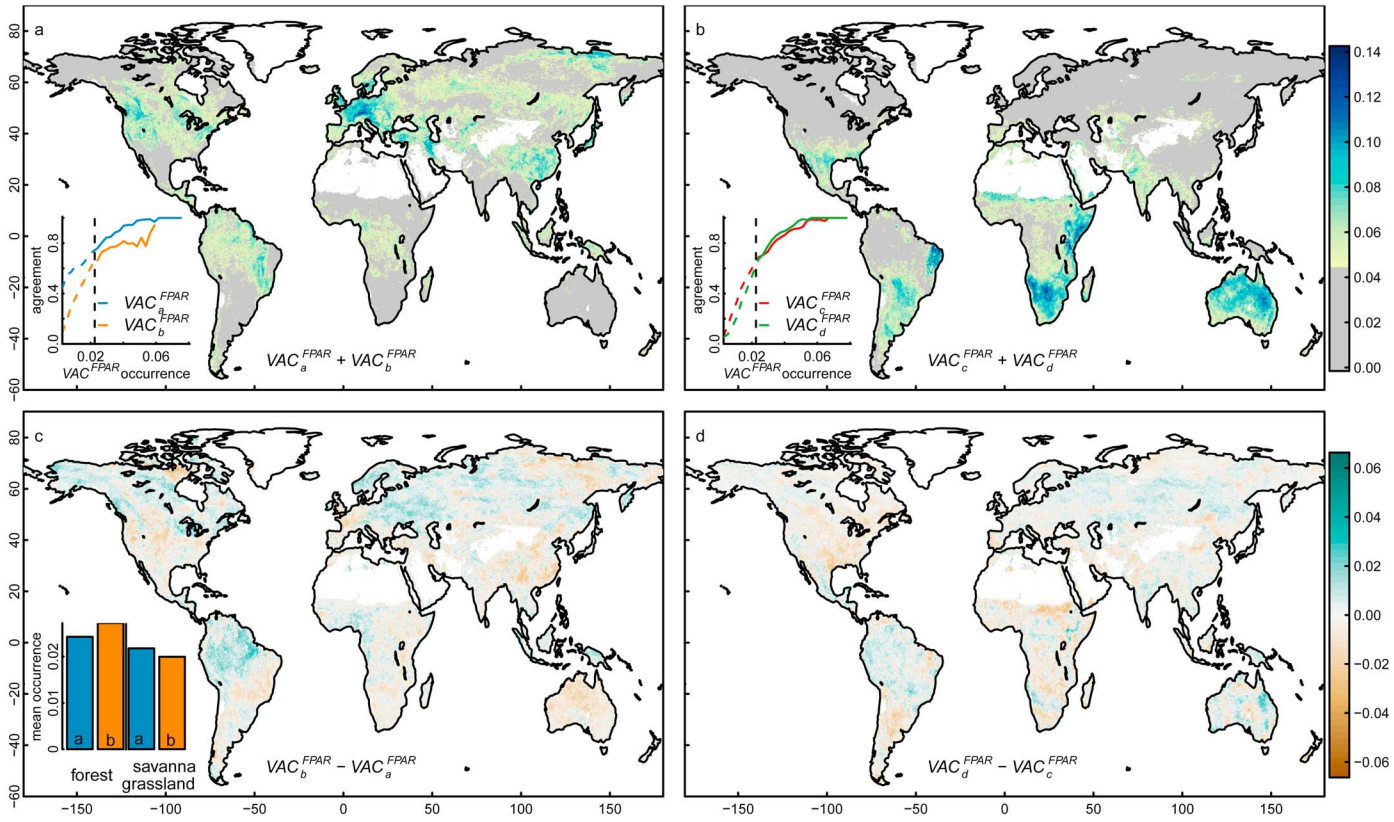

Figure 2. (a, b) Probability of occurrence of $VAC_a^{FPAR} + VAC_b^{FPAR}$ and $VAC_c^{FPAR} + VAC_d^{FPAR}$, respectively. Areas where the index does not exceed random occurrence (assuming T and FPAR were independent and symmetric, a random occurrence of $2 \times 0.15^2 = 0.045$ is expected) are shaded in grey. Insets show fraction of pixels with agreement between VAC^{FPAR} and VAC^{ET} significantly higher than chance level ($p < 0.05$) as a function of per pixel occurrence rate of VAC^{FPAR} for each subclass. The vertical dashed line denotes the significance level ($0.15^2 = 0.0225$). (c, d) Difference between probability of occurrence between VAC_b^{FPAR} and VAC_a^{FPAR} and VAC_d^{FPAR} and VAC_c^{FPAR}, respectively. Inset in Figure 2c shows the average occurrence rates of VAC_a^{FPAR} and VAC_b^{FPAR} in forests as well as savannas and grasslands using Moderate Resolution Imaging Spectroradiometer land cover [*Channan et al.*, 2014].

between ET and radiation. Higher T in VAC_b^{FPAR} is associated with higher radiation, but the increase in ET is not proportional, leading to lower EF. Incidences of VAC_c^{FPAR} and VAC_d^{FPAR} are aligned along a gradient from low SM/low EF to high SM/high EF, illustrating a relationship between EF and SM which is indicative of a transitional regime [*Seneviratne et al.*, 2010]. While this behavior is expected, such a good alignment is nevertheless noteworthy since the derivation of the FPAR-T data is largely independent of the SM, ET, and net radiation products. This demonstrates the usefulness of the VAC^{FPAR} index for identifying different evaporative regimes as well as transitions between them. Note that we cannot test for causal relationships in our framework. This would require a model-based approach.

These results can help to derive a SM threshold which separates the transitional from the energy-limited regime. Characterization of such a threshold is important for diagnosing and predicting periods during which heat waves can potentially be aggravated by SM-T feedbacks [e.g., *Mueller and Seneviratne*, 2012; *Quesada et al.*, 2012]. Using SM data for Europe by *Orth and Seneviratne* [2015], we find here a SM threshold of approximately 700 to 800 mm or a deficit of 170 to 270 mm compared to the water holding capacity of the underlying model (970.5 mm) [*Orth and Seneviratne*, 2015]. Note that we expect the absolute threshold to be strongly model dependent but the relative threshold to be more robust across products [*Koster et al.*, 2009]. In a similar way by analyzing the relationship between annual precipitation and ET or photosynthetic activity, annual precipitation thresholds of around 1900–2000 mm have been identified to distinguish tropical forest from savanna in Brazil [*da Rocha et al.*, 2009] and whether tropical forests are water limited during dry season [*Guan et al.*, 2015].

3.2. Identification of Energy- and Water-Limited Regimes

A control of land surface processes on atmospheric processes is only expected in transitional SM regimes [*Seneviratne et al.*, 2010]. The regimes VAC_a^{FPAR} and VAC_b^{FPAR} (T and FPAR anomalies have the same sign) indicate

that atmospheric forcing (T, radiation, and precipitation) dominates processes at the land surface, including vegetation activity (i.e., FPAR). This is generally expected in energy-limited and thus humid areas [see also *Seneviratne et al.*, 2006]. The probability of occurrence of classes VAC_a^{FPAR} and VAC_b^{FPAR} in Figure 2a shows that in humid regimes [*Thornthwaite*, 1948; *Greve et al.*, 2014] anomalies in FPAR and T are often aligned (cf. Figure 1a), pointing toward an atmospheric control of land-climate coupling [*Seneviratne et al.*, 2006]. Classes VAC_c^{FPAR} and VAC_d^{FPAR} on the other hand (T and FPAR anomalies have opposite sign) occur more often in semiarid and arid areas (Figure 2b). Here precipitation spells (and consequently lower T [*Berg et al.*, 2015]) lead to a spontaneous greening of the vegetation, thus increasing FPAR (VAC_d^{FPAR}; see, e.g., Figure S3). Dry periods, on the other hand, are associated with precipitation deficit and/or low SM, forcing plants to close their stomata and thus decreasing FPAR (VAC_c^{FPAR}). In this regime, SM has a strong control upon ET and T (Figure 1a) [*Seneviratne et al.*, 2006]. Because the VAC index is based on anomalies, we can conclude that arid and semiarid regions are characterized by frequent and irregular occurrences of vegetation stress (VAC_c^{FPAR}) and greening (VAC_d^{FPAR}), mostly driven by water availability [*Wang and Dickinson*, 2012]. In this way, water availability contributes substantially to the interannual variability of the global carbon cycle [*Zscheischler et al.*, 2014a, 2014b; *Ahlström et al.*, 2015].

The classes VAC_a^{FPAR} and VAC_b^{FPAR}, and respectively VAC_c^{FPAR} and VAC_d^{FPAR}, do not occur with the same frequency at each pixel. Periods with enhanced T and FPAR (VAC_b^{FPAR}) occur up to 6% more often compared to periods where T and FPAR are decreased (VAC_a^{FPAR}) in the Amazon, eastern Europe, western central Africa, and parts of Russia and Canada (Figure 2c). These areas generally coincide with the distribution of forests [*Friedl et al.*, 2002]. Periods where T and FPAR are decreased occur more often in the U.S., Brazil, Australia, China, and central Europe, which are regions where grasslands and savannas dominate [*Friedl et al.*, 2002] (see also inset in Figure 2c). This asymmetry could indicate that forests, which are found in rather energy-limited areas, have the capacities to photosynthesize more carbon if more energy is available and are less sensitive to below normal energy availability. In contrast, savannas and grasslands are usually more dependent on precipitation [*Knapp and Smith*, 2001] and might be optimized to the normally available energy, thus reacting more strongly to below normal energy. Such an asymmetry is not apparent in the transitional regime. Overall, the difference map between VAC_c^{FPAR} and VAC_d^{FPAR} reveals a more mixed picture, indicating that both vegetation greening and vegetation stress occur similarly often. Periods of greening (VAC_d^{FPAR}) occur more often in the Amazon, Central America, Russia, and some parts of Australia and Africa. Periods of vegetation stress (VAC_c^{FPAR}) occur more often in Eastern North America, Southern South America, Northeastern Brazil, the Sahel, and some parts of Southern Africa, Australia, and the Middle East.

3.3. Can ET and FPAR Be Used Interchangeably for the VAC Index?

The two indices VAC^{FPAR} and VAC^{ET} are strongly correlated, in particular in regions where the classes of VAC^{FPAR} occur frequently. The insets in Figures 2a and 2b relate the number of pixels with significant co-occurrences between VAC^{FPAR} and VAC^{ET} with the frequency of occurrence of classes in VAC^{FPAR}. For regions where VAC^{FPAR} has significant occurrence rates, VAC^{FPAR} and VAC^{ET} co-occur significantly more often than random on at least 70% of the affected pixels, underlining the strong coupling between vegetation activity and ET, particularly during extreme conditions [e.g., *Schwalm et al.*, 2012]. ET measurements are not available for longer time scales and large spatial scales; hence, to study land-atmosphere coupling, one usually has to rely on model output. Here we illustrate that FPAR can be used as an alternative.

3.4. Case Studies

Western Russia and the Amazon are humid areas [*Greve et al.*, 2014] in which vegetation activity is generally not constrained by SM; i.e., they exhibit few occurrences of VAC_c and VAC_d (Figure 2b). However, in periods of drought SM can become the limiting factor such that the relationship between T and FPAR/ET becomes anticorrelated, that is, a transition to class VAC_c. We discuss this behavior at two examples, the Russian heat wave in 2010 and the Amazon drought of 2010.

3.4.1. Russian 2010 Heat Wave

During the Russian heat wave in summer 2010 the 15 day mean of maximum T exceeded 5 standard deviations compared to 1970–1999 for some areas [*Barriopedro et al.*, 2011]. At the same time, dry SM anomalies exceeded 2 standard deviations in large areas across western Russia [*Orth and Seneviratne*, 2015]. This had serious impacts on vegetation [*Yoshida et al.*, 2015]. Although occurrences of VAC_c^{FPAR} are very rare in the northern midlatitudes (Figure 2b), the Russian heat wave led to a large contiguous area ($> 1,000,000$ km^2) in the first half of August where T anomalies are above 2 and FPAR anomalies are below 2 standard deviations at the same time (Figure 3). Comparing with the entire VAC^{FPAR} inventory, we found that vegetation stress of this spatial

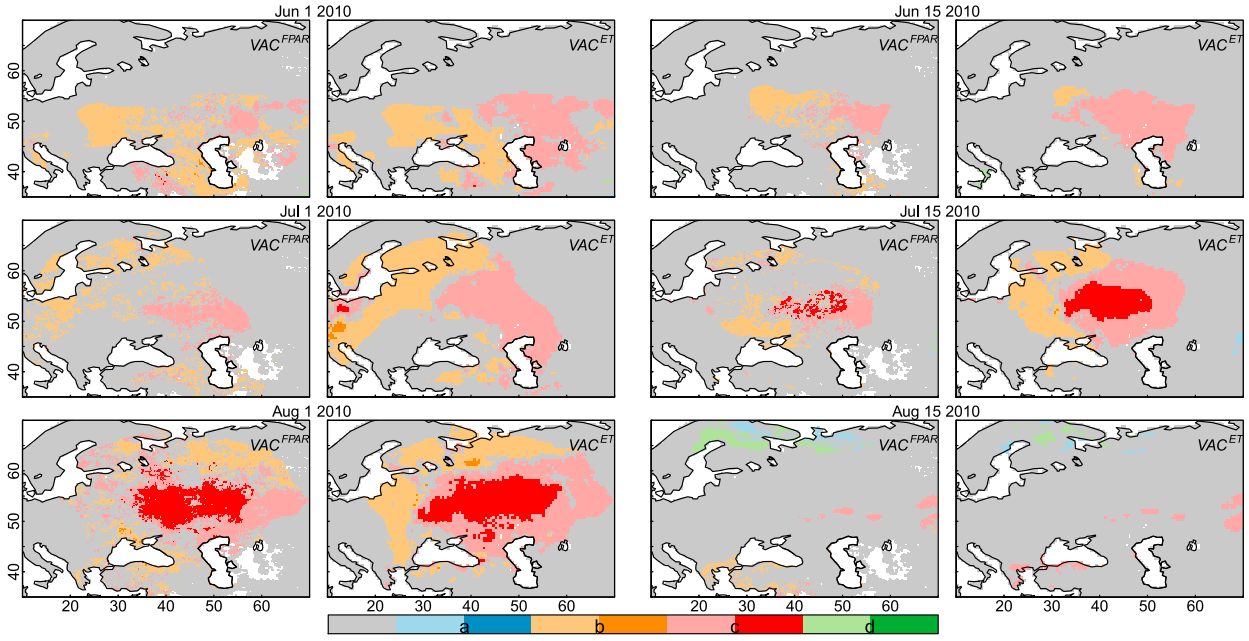

Figure 3. Development of the 2010 heat wave in Russia (June to August) displayed in terms of (first and third columns) VAC^{FPAR} and (second and fourth columns) VAC^{ET}. Colors are according to Table 1.

extent is unprecedented on the Northern Hemisphere. In fact, this is the largest spatiotemporally contiguous occurrence of class VAC_c^{FPAR} in the Northern Hemisphere between 1982 and 2011 (spatiotemporal coherence assessed with the method of *Zscheischler et al.* [2013]).

Both VAC^{FPAR} and VAC^{ET} show occurrences of VAC_b and VAC_c in the area already beginning of June (Figure 3). While in some areas in the west SM is high enough to support increased vegetation activity with high temperatures (VAC_b), in the east of the domain soils are too dry, leading to decreased FPAR and ET (VAC_c) (Figure S4). However, only at the end of July the indexes start to cross the 95% threshold for VAC_c, reaching the maximum extent beginning of August with no more occurrences in the second half of August. VAC^{FPAR} and VAC^{ET}

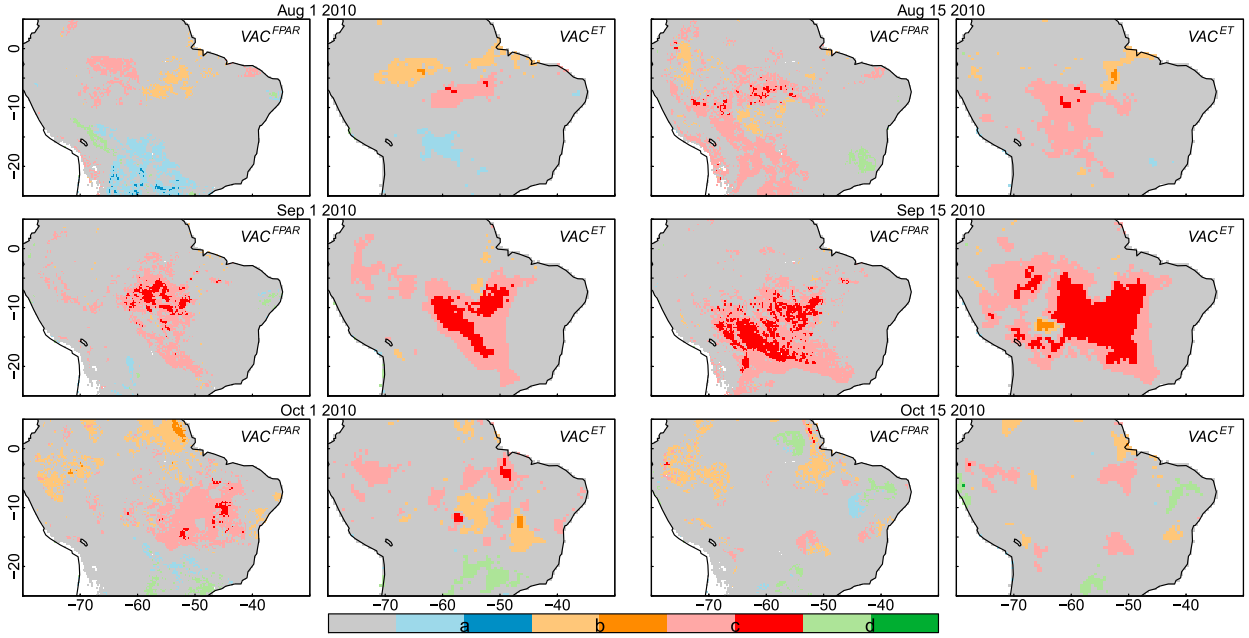

Figure 4. As in Figure 3 but for the 2010 drought in the Amazon (August to September).

agree well during summer 2010 although VAC^{ET} has smoother patterns, probably because the underlying ET is mainly estimated by land surface models.

3.4.2. Amazon 2010 Drought

In the same year the Amazon region was hit by an extreme drought with a dry-season rainfall that was 2 standard deviations lower than normal for a large area [*Lewis et al.*, 2011] and consequently strongly decreased vegetation activity [*Xu et al.*, 2011]. In Figure 4 we compare VAC^{FPAR} and VAC^{ET} over the northern part of South America between August and September 2010. Larger-scale occurrences of VAC_c start in the second half of August and intensify until the end of September for the southern Amazon. VAC_c covers less area beginning of October before it disappears in the second half of October. As during the Russian heat wave, VAC^{FPAR} and VAC^{ET} are highly correlated with smoother patterns for VAC^{ET}.

4. Conclusions

We introduce the VAC index to detect co-occurrences between strong *T* and FPAR anomalies at high spatial and temporal resolution. With the VAC index, periods of strong coupling between *T* and vegetation activity can be detected. Moreover, changes between transitional and energy-limited evaporative regimes can be identified, and thus, an indirect information about the local SM state can be obtained.

Using the 2010 heat wave in Europe and the 2010 Amazon drought as examples, we illustrate how the VAC index can help to understand the development of extreme climate events and their impacts on vegetation at high spatial and temporal resolution. Exchanging FPAR with ET leads to qualitatively similar results, emphasizing the strong coupling between photosynthetic activity and the water cycle during extreme conditions. The framework can be easily applied to long-term point-scale observations of T, ET, and FPAR, and other vegetation properties such as the normalized difference vegetation index and gross primary production.

Overall, the VAC index is a useful tool to detect when a region tips from an energy-limited regime to a water-limited regime. It helps to identify periods of vegetation stress and quantify stress intensity through the different levels of the index which can be chosen by the user, demonstrating the universal applicability if the VAC index. Identifying such transitions is important for understanding under which circumstances vegetation is water stressed and can be used to diagnose changes in vegetation stress in future projections.

Acknowledgments

This work was partially supported by the ERC DROUGHT-HEAT project (grant agreement 617518). We thank Richard Wartenburger for downloading the used data sets. We acknowledge the eartH2Observe project for providing model-based ET products (https://wci.earth2observe.eu/). We thank Ranga Myneni for providing the FPAR3g data.

References

Ahlström, A., et al. (2015), The dominant role of semi-arid ecosystems in the trend and variability of the land CO_2 sink, *Science*, *348*(6237), 895–899, doi:10.1126/science.aaa1668.

Barriopedro, D., E. M. Fischer, J. Luterbacher, R. M. Trigo, and R. García-Herrera (2011), The hot summer of 2010: Redrawing the temperature record map of Europe, *Science*, *332*(6026), 220–224.

Berg, A., et al. (2015), Interannual coupling between summertime surface temperature and precipitation over land: Processes and implications for climate change, *J. Clim.*, *28*(3), 1308–1328.

Channan, S., K. Collins, and W. Emanuel (2014), *Global Mosaics of the Standard MODIS Land Cover Type Data*, Univ. of Maryland and the Pacific Northwest National Laboratory, College Park, Md.

da Rocha, H. R., et al. (2009), Patterns of water and heat flux across a biome gradient from tropical forest to savanna in Brazil, *J. Geophys. Res.*, *114*, G00B12, doi:10.1029/2007JG000640.

Dee, D., et al. (2011), The ERA-Interim reanalysis: Configuration and performance of the data assimilation system, *Q. J. R. Meteorol. Soc.*, *137*(656), 553–597.

Ford, T. W., and S. M. Quiring (2013), Influence of MODIS-derived dynamic vegetation on VIC-simulated soil moisture in Oklahoma, *J. Hydrometeorol.*, *14*(6), 1910–1921.

Frank, D., et al. (2015), Effects of climate extremes on the terrestrial carbon cycle: Concepts, processes and potential future impacts, *Global Change Biol.*, *21*, 2861–2880, doi:10.1111/gcb.12916.

Friedl, M., et al. (2002), Global land cover mapping from MODIS: Algorithms and early results, *Remote Sens. Environ.*, *83*(1–2), 287–302.

Gobron, N., A. Belward, B. Pinty, and W. Knorr (2010), Monitoring biosphere vegetation 1998–2009, *Geophys. Res. Lett.*, *37*, L15402, doi:10.1029/2010GL043870.

Good, S. P., D. Noone, and G. Bowen (2015), Hydrologic connectivity constrains partitioning of global terrestrial water fluxes, *Science*, *349*(6244), 175–177.

Greve, P., B. Orlowsky, B. Mueller, J. Sheffield, M. Reichstein, and S. I. Seneviratne (2014), Global assessment of trends in wetting and drying over land, *Nat. Geosci.*, *7*(10), 716–721.

Guan, K., et al. (2015), Photosynthetic seasonality of global tropical forests constrained by hydroclimate, *Nat. Geosci.*, *8*(4), 284–289.

Guillod, B. P., B. Orlowsky, D. G. Miralles, A. J. Teuling, and S. I. Seneviratne (2015), Reconciling spatial and temporal soil moisture effects on afternoon rainfall, *Nat. Commun.*, *6*, 6443, doi:10.1038/ncomms7443.

Hirschi, M., S. I. Seneviratne, V. Alexandrov, F. Boberg, C. Boroneant, O. B. Christensen, H. Formayer, B. Orlowsky, and P. Stepanek (2011), Observational evidence for soil-moisture impact on hot extremes in southeastern Europe, *Nat. Geosci.*, *4*(1), 17–21.

Knapp, A. K., and M. D. Smith (2001), Variation among biomes in temporal dynamics of aboveground primary production, *Science*, *291*(5503), 481–484.

Knorr, W., N. Gobron, M. Scholze, T. Kaminski, R. Schnur, and B. Pinty (2007), Impact of terrestrial biosphere carbon exchanges on the anomalous CO_2 increase in 2002–2003, *Geophys. Res. Lett.*, *34*(9).

Koster, R. D., and P. Milly (1997), The interplay between transpiration and runoff formulations in land surface schemes used with atmospheric models, *J. Clim.*, *10*(7), 1578–1591.
Koster, R. D., et al. (2004), Regions of strong coupling between soil moisture and precipitation, *Science*, *305*(5687), 1138–1140.
Koster, R. D., Z. Guo, R. Yang, P. A. Dirmeyer, K. Mitchell, and M. J. Puma (2009), On the nature of soil moisture in land surface models, *J. Clim.*, *22*(16), 4322–4335.
Lawrence, D. M., et al. (2011), Parameterization improvements and functional and structural advances in version 4 of the Community Land Model, *J. Adv. Model. Earth Syst.*, *3*, M03001, doi:10.1029/2011MS000045.
Lewis, S. L., P. M. Brando, O. L. Phillips, G. M. F. van der Heijden, and D. Nepstad (2011), The 2010 Amazon drought, *Science*, *331*(6017), 554, doi:10.1126/science.1200807.
Lorenz, R., E. B. Jaeger, and S. I. Seneviratne (2010), Persistence of heat waves and its link to soil moisture memory, *Geophys. Res. Lett.*, *37*, L09703, doi:10.1029/2010GL042764.
Miralles, D. G., A. J. Teuling, C. C. van Heerwaarden, and J. V.-G. de Arellano (2014), Mega-heatwave temperatures due to combined soil desiccation and atmospheric heat accumulation, *Nat. Geosci.*, *7*(5), 345–349.
Mueller, B., and S. I. Seneviratne (2012), Hot days induced by precipitation deficits at the global scale, *Proc. Natl. Acad. Sci. U.S.A.*, *109*(31), 12,398–12,403.
Mueller, B., et al. (2013), Benchmark products for land evapotranspiration: LandFlux-EVAL multi-data set synthesis, *Hydrol. Earth Syst. Sci.*, *17*, 3707–3720.
Oglesby, R. J., and D. J. Erickson III (1989), Soil moisture and the persistence of North American drought, *J. Clim.*, *2*(11), 1362–1380.
Orth, R., and S. I. Seneviratne (2015), Introduction of a simple-model-based land surface dataset for Europe, *Environ. Res. Lett.*, *10*(4), 44,012, doi:10.1088/1748-9326/10/4/044012.
Pinty, B., T. Lavergne, J.-L. Widlowski, N. Gobron, and M. Verstraete (2009), On the need to observe vegetation canopies in the near-infrared to estimate visible light absorption, *Remote Sens. Environ.*, *113*(1), 10–23, doi:10.1016/j.rse.2008.08.017.
Quesada, B., R. Vautard, P. Yiou, M. Hirschi, and S. I. Seneviratne (2012), Asymmetric European summer heat predictability from wet and dry southern winters and springs, *Nat. Clim. Change*, *2*(10), 736–741.
Reichstein, M., et al. (2013), Climate extremes and the carbon cycle, *Nature*, *500*(7462), 287–295.
Schlesinger, W. H., and S. Jasechko (2014), Transpiration in the global water cycle, *Agric. Forest Meteorol.*, *189*, 115–117.
Schwalm, C. R., et al. (2012), Reduction in carbon uptake during turn of the century drought in western North America, *Nat. Geosci.*, *5*(8), 551–556.
Seneviratne, S. I., D. Lüthi, M. Litschi, and C. Schär (2006), Land-atmosphere coupling and climate change in Europe, *Nature*, *443*(7108), 205–209.
Seneviratne, S. I., T. Corti, E. L. Davin, M. Hirschi, E. B. Jaeger, I. Lehner, B. Orlowsky, and A. J. Teuling (2010), Investigating soil moisture-climate interactions in a changing climate: A review, *Earth Sci. Rev.*, *99*(3), 125–161.
Suzuki, R., K. Masuda, and D. G. Dye (2007), Interannual covariability between actual evapotranspiration and PAL and GIMMS NDVIs of northern Asia, *Remote Sens. Environ.*, *106*(3), 387–398.
Taylor, C. M., R. A. de Jeu, F. Guichard, P. P. Harris, and W. A. Dorigo (2012), Afternoon rain more likely over drier soils, *Nature*, *489*(7416), 423–426.
Teuling, A. J., et al. (2009), A regional perspective on trends in continental evaporation, *Geophys. Res. Lett.*, *36*, L02404, doi:10.1029/2008GL036584.
Teuling, A. J., et al. (2010), Contrasting response of European forest and grassland energy exchange to heatwaves, *Nat. Geosci.*, *3*(10), 722–727.
Thornthwaite, C. (1948), An approach toward a rational classification of climate, *Geogr. Rev.*, *38*(1), 55–94.
Wang, K., and R. E. Dickinson (2012), A review of global terrestrial evapotranspiration: Observation, modeling, climatology, and climatic variability, *Rev. Geophys.*, *50*, RG2005, doi:10.1029/2011RG000373.
Whan, K., J. Zscheischler, R. Orth, M. Shongwe, M. Rahimi, E. O. Asare, and S. I. Seneviratne (2015), Impact of soil moisture on extreme maximum temperatures in Europe, *Weather Clim. Extremes*, *9*, 57–67.
Xu, L., A. Samanta, M. H. Costa, S. Ganguly, R. R. Nemani, and R. B. Myneni (2011), Widespread decline in greenness of Amazonian vegetation due to the 2010 drought, *Geophys. Res. Lett.*, *38*, L07402, doi:10.1029/2011GL046824.
Yoshida, Y., et al. (2015), The 2010 Russian drought impact on satellite measurements of solar-induced chlorophyll fluorescence: Insights from modeling and comparisons with parameters derived from satellite reflectances, *Remote Sens. Environ.*, *166*, 163–177.
Zhu, Z., et al. (2013), Global data sets of vegetation leaf area index (LAI) 3g and Fraction of Photosynthetically Active Radiation (FPAR) 3g derived from Global Inventory Modeling and Mapping Studies (GIMMS) Normalized Difference Vegetation Index (NDVI3g) for the period 1981 to 2011, *Remote Sens.*, *5*(2), 927–948.
Zscheischler, J., M. D. Mahecha, S. Harmeling, and M. Reichstein (2013), Detection and attribution of large spatiotemporal extreme events in Earth observation data, *Ecol. Inf.*, *15*, 66–73.
Zscheischler, J., et al. (2014a), A few extreme events dominate global interannual variability in gross primary production, *Environ. Res. Lett.*, *9*, 35001, doi:10.1088/1748-9326/9/3/035001.
Zscheischler, J., M. Reichstein, S. Harmeling, A. Rammig, E. Tomelleri, and M. D. Mahecha (2014b), Extreme events in gross primary production: A characterization across continents, *Biogeosciences*, *11*, 2909–2924.